

pH Modulated Heterogeneous Electron Transfer across Metal/Monolayer Interfaces

Robert J. Forster* and Joseph P. O'Kelly

School of Chemical Sciences, Dublin City University, Dublin 9, Ireland

Received: July 21, 1995; In Final Form: October 15, 1995[⊗]

Dense monolayers of $[\text{Os}(\text{bpy})_2(\text{p3p})_2]^{2+}$, where bpy is 2,2'-bipyridyl and p3p is 4,4'-trimethylenedipyridine, have been formed by spontaneous adsorption onto clean platinum microelectrodes. Cyclic voltammetry of these monolayers is nearly ideal, and the area occupied per molecule suggests that only one of the p3p ligands binds to the electrode surface, the other being available for protonation. Chronoamperometry conducted on a microsecond time scale has been used to measure the heterogeneous electron transfer rate constant k for the $\text{Os}^{2+/3+}$ redox reaction. For electrolyte concentrations above 0.1 M, heterogeneous electron transfer is characterized by a single unimolecular rate constant (k/s^{-1}). Tafel plots of the dependence of $\ln k$ on the overpotential η show curvature, and larger cathodic than anodic rate constants are observed for a given absolute value of η . This response is consistent with electron transfer occurring via a through-space tunneling mechanism. Plots of k vs pH are sigmoidal, and the standard heterogeneous rate constant k° decreases from $(6.1 \pm 0.2) \times 10^4$ to $(1.6 \pm 0.1) \times 10^4 \text{ s}^{-1}$ as the pH of the contacting solution is decreased from 5.05 to 1.07. When in contact with pH 5.05 electrolyte, the electrochemical enthalpy ΔH^\ddagger is $37.5 \pm 2.1 \text{ kJ mol}^{-1}$, which decreases to $24.6 \pm 1.5 \text{ kJ mol}^{-1}$ at a pH of 1.07. The reaction entropy $\Delta S_{\text{rc}}^\circ$ is independent of the pH over this range, maintaining a value of $82 \pm 7 \text{ J mol}^{-1} \text{ K}^{-1}$. In contrast to the behavior expected from the decrease of k with decreasing pH, the free energy of activation ΔG^\ddagger decreases with decreasing pH. The electronic transmission coefficient κ_{el} , describing the probability of electron transfer once the nuclear transition state has been reached, is considerably less than unity for all pH's investigated. κ_{el} decreases with decreasing solution pH, suggesting an increasingly weaker electronic interaction between the metallic states of the electrode and the orbitals of the redox center as the monolayer becomes protonated. These results suggest that monolayer protonation modulates the heterogeneous electron transfer rate by changing the through-space electron transfer distance. This may be caused either by a change in the tilt angle between the adsorbate and the electrode or by the methylene spacer units within the bridging ligand becoming extended, when the monolayer is protonated.

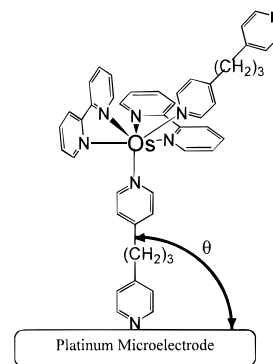
Introduction

The field of molecular electronics ranges from well-defined and well-understood phenomena such as nonlinear optical responses to the tantalizing, and conceptually more difficult, areas of computing and information storage at the molecular level.¹ Supramolecular assemblies, constructed using single electroactive molecules as building blocks, offer a striking way to create electrically conducting materials whose organized architecture makes them suitable for developing molecular electronic devices.

Progress toward this strategic goal demands not only the development of new synthetic approaches that yield highly ordered materials² but also careful attention to those elementary processes that dictate the rate of heterogeneous electron transfer across metal/monolayer interfaces.³ However, it is only recently that it has been possible to *directly* probe those factors that govern the rate of electron transfer processes that are complete within a few billionths of a second. In fact, coupling recent advances in the design and fabrication of microelectrodes and electrochemical instrumentation that operate on a nanosecond time scale with chemical systems that are organized on a molecular level, promises to revolutionize investigations into electron transfer processes.⁴

Toward the objective of understanding those factors that influence heterogeneous electron transfer, we have formed osmium containing monolayers by spontaneously adsorbing $[\text{Os}(\text{bpy})_2(\text{p3p})_2]^{2+}$ complexes (Chart 1), where bpy is 2,2'-

CHART 1



bipyridyl and p3p is 4,4'-trimethylenedipyridine, onto clean platinum microelectrodes. For simplicity, we denote these monolayers as $(\text{p3p})_2$. These adsorbed monolayers are stable for long periods at elevated temperatures in aqueous perchlorate solutions allowing those factors that control the rate and pathway for electron transfer across metal/monolayer interfaces to be probed in considerable detail. Moreover, it appears that only one of the pyridine groups binds to the electrode surface, while the other is available for protonation, thus allowing chemical effects on heterogeneous electron transfer to be explored.

We have used chronoamperometry, performed on a microsecond time scale, to probe the structure of the modified interface, focusing particularly on the extent to which solvent and ions permeate the interior of the monolayer. These investigations are doubly important, since they provide an insight into the relative perfection of the monolayer and allow one to

* To whom correspondence should be addressed.

⊗ Abstract published in *Advance ACS Abstracts*, January 15, 1996.

probe the interfacial potential distribution.⁵ High-speed chronoamperometry has also been used to investigate the dynamics of heterogeneous electron transfer across the electrode/monolayer interface. When the supporting electrolyte concentration is greater than about 0.1 M, these chronoamperometric responses are remarkably well-behaved, with heterogeneous electron transfer being characterized by a single rate constant over more than two lifetimes.

Significantly, the solution pH modulates the rate of heterogeneous electron transfer, apparently by protonating the pyridine moiety of the unbound p3p ligand. We have probed the origin of this pH sensitivity by systematically probing the pH dependence of the free energy of activation ΔG^\ddagger and the degree of electronic coupling between the remote redox centers and the electrode. Surprisingly, our investigation suggests that changes in the pre-exponential factor with pH rather than the activation barrier cause the heterogeneous electron transfer rate constant to depend on the extent of monolayer protonation.

Investigations of this type are especially important for improving our understanding of those processes that limit the rate of electron transfer within biological systems where subtle changes in the chemical microenvironment surrounding the redox site can dramatically alter the electron transfer rates.⁶

Experimental Section

Materials. The surface active complex, $[\text{Os}(\text{bpy})_2(\text{p3p})_2]^{2+}$, was prepared by first placing 50 mg (0.09 mmol) of $[\text{Os}(\text{bpy})_2\text{Cl}_2]$ in 40 cm³ of methanol followed by 10 min reflux to ensure complete dissolution. A solution of 70 mg (0.036 mmol) of 4,4'-trimethylenedipyridine (98%, Aldrich) dissolved in 5 cm³ of methanol, together with 150 cm³ of milli-Q water were added, and the resulting solution was refluxed for 15 h. After approximately 10–12 h the color of the solution changed from red-brown to dark green. The progress of the reaction was monitored using HPLC and cyclic voltammetry. After the reaction was complete, the volume was reduced to 5 cm³ by rotary evaporation. Ammonium hexafluorophosphate (95+%, Aldrich) was then added, and the dark green product was collected by filtration and washed with diethyl ether. The product was recrystallized from aqueous methanol to give dark green-black crystals, yield 66 mg, 82%. The complex was characterized using IR, UV-vis, NMR, and cyclic voltammetry.

Apparatus. Electrochemical cells were of conventional design and were thermostated within ± 0.2 °C using a Julabo F10-HC refrigerated circulating bath. All potentials are quoted with respect to a BAS Ag/AgCl gel-filled reference electrode, the potential of which was 35 mV more positive than that of the saturated calomel electrode (SCE). Cyclic voltammetry was performed using an EG&G Model 273 potentiostat/galvanostat and a conventional three-electrode cell. All solutions were degassed using nitrogen, and a blanket of nitrogen was maintained over the solution during all experiments. The degree of monolayer protonation was altered by systematically varying the pH of the contacting electrolyte solution over the range 5.1 to 1.1 by addition of concentrated HClO₄ to LiClO₄ solutions. These solutions were not pH buffered to avoid difficulties with competitive adsorption effects from buffer ions.

As described previously,⁷ a custom built function generator–potentiostat, with a rise time of less than 10 ns, was used to apply potential steps of variable pulse width and amplitude directly to a two-electrode cell. A Pt foil and an Ag/AgCl reference electrode were combined to form a counter electrode. The foil lowered the resistance and provided a high-frequency path.

For the temperature resolved experiments, a nonisothermal cell was used in which the reference electrode was isolated from

the main compartment by a salt bridge and held at constant temperature. The nonisothermal salt bridge contained saturated KCl since it has a low resistance, and the salt remains soluble at the lowest temperature employed (–5 °C). The high electrolyte concentration and the design of the bridge minimize any systematic error in the reported temperature effects on E°' due to changes in the liquid junction potential with temperature.⁸

Microelectrodes were fabricated from platinum microwires (Goodfellow Metals Ltd.) of radii between 5 and 25 μm by sealing them in soft glass using a procedure described previously.^{4b,9} Microdisk electrodes were exposed by removing excess glass using 600 grit emery paper followed by successive polishing with 12.5, 5, 1, 0.3, and 0.05 μm alumina. The polishing material was removed between changes of particle size by sonicating the electrodes in deionized water for at least 5 min. The polished electrodes were electrochemically cleaned by cycling in 0.1 M HClO₄ between potential limits chosen to first oxidize and then to reduce the surface of the platinum electrode. Excessive cycling was avoided in order to minimize the extent of surface roughening. Finally, the electrode was cycled between –0.300 and +0.900 V in 0.1 M NaClO₄ until hydrogen desorption was complete.

The real surface area of the electrodes was found by calculating the charge under the oxide or hydrogen adsorption–desorption peaks.¹⁰ Typically, the surface roughness factor was between 1.3 and 1.6. Obtaining the real, as opposed to the projected or geometric, surface area of the electrodes is important if the area occupied per molecule is to be accurately measured.

RC cell time constants, measured in blank electrolyte solution, were between 0.03 and 3 μs , depending on the electrode radius and the supporting electrolyte concentration. The interfacial kinetics were measured only at times greater than about 5–10 RC. In chronoamperometry experiments, the initial potential was either 0.000 or +1.000 V, depending on whether oxidation or reduction kinetics were being probed.

Spontaneously adsorbed monolayers were typically formed by immersing the electrodes in a methanol/water solution of the metal complex for 8–12 h. No precautions were taken to exclude oxygen during monolayer formation. Before electrochemical measurements were made, the modified electrodes were rinsed with the electrochemical solvent to remove unbound material. Subsequent measurements were performed in blank electrolyte solutions.

Results and Discussion

General Electrochemical Properties. Figure 1 shows representative cyclic voltammograms for a spontaneously adsorbed (p3p)₂ monolayer, where the supporting electrolyte is 0.1 M LiClO₄ (pH = 4.8) that does not contain any dissolved $[\text{Os}(\text{bpy})_2(\text{p3p})_2]^{2+}$. This voltammetric response is consistent in all respects with that expected for an electrochemically reversible reaction involving a surface-confined species.¹¹ For example, the peak shapes are independent of scan rate, at least over the range of 1–50 V/s, and the peak height scales linearly with the scan rate v , unlike the $v^{1/2}$ dependence expected for a freely diffusing species. Therefore, it appears that the osmium complex adsorbs onto the surface of the platinum microelectrode to give an electroactive film. Where there are no lateral interactions between surface confined redox centers and a rapid equilibrium is established with the electrode, a zero peak-to-peak splitting (ΔE_p) and a fwhm of 90.6 mV are expected for a reaction involving the transfer of a single electron. As discussed previously for $[\text{Os}(\text{bpy})_2\text{Cl}(\text{pNp})]^+$ monolayers,⁷ where pNp is 4,4'-bipyridyl or 1,2-dipyridylethane, we consis-

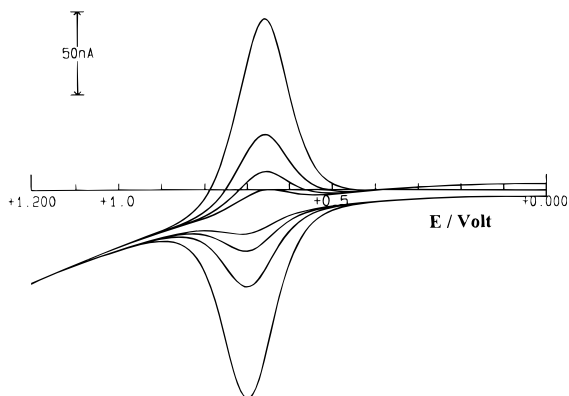


Figure 1. Scan rate dependence of cyclic voltammetry for a spontaneously adsorbed (p3p)₂ monolayer. The scan rates are (top to bottom) 50, 20, 10, and 5 V/s. The surface coverage is 9.8×10^{-11} mol cm⁻². The supporting electrolyte is 0.1 M LiClO₄ at a pH of 4.8. The radius of the platinum microelectrode is 25 μm. The cathodic currents are up, and the anodic currents are down. Each cycle begins at the negative limit.

tently observe a nonzero ΔE_p , even at low scan rates; e.g., ΔE_p is 12 ± 3 mV at a scan rate of 500 mV/s. Feldberg has interpreted nonzero peak-to-peak splitting in terms of unusual quasi-reversibility (UQR).¹² In this model, hysteresis is observed in cyclic voltammetry because some rate processes, e.g., heterogeneous electron transfer, ion movement, changes in monolayer structure that accompany redox switching, etc., are slow compared to the time scale of the experiment. We do not consider this issue in detail here except to note that neither heterogeneous electron transfer or double layer assembly (vide infra) limit the voltammetric response at these scan rates. In general, the voltammetric response is consistent with that expected for a rapid, reversible electron transfer to an immobilized redox active species. The peak height and peak area of the voltammograms do not change by more than 15% when cycled repeatedly over an 10 h period at temperatures up to 40 °C, indicating that the monolayers are both electrochemically and thermally stable. We observe only a 20–30 mV difference between the formal potentials of the solution-phase model compound, [Os(bpy)₃]²⁺, and the monolayer, suggesting that the redox centers within the monolayer are solvated.

The total charge introduced or withdrawn to reduce or oxidize the monolayer can be found from the area under the voltammetric peak after correcting for the background charging current. This charge, together with the real surface area, can then be used to calculate the surface coverage, or the number of moles of [Os(bpy)₂(p3p)₂]²⁺ per cm². The surface coverage provides important information about the packing density of the monolayer and may provide a limited insight into the way that the complex adsorbs onto the electrode surface. This is important since the cis configuration of the bpy ligands makes it possible for adsorption to occur through one or both of the p3p ligands.

The surface coverage, Γ , as experimentally determined from the area under the cyclic voltammetric wave, was found to be $(1.05 \pm 0.08) \times 10^{-10}$ mol cm⁻², corresponding to an area occupied per molecule of 166 ± 12 Å². When the additional contributions to the molecular volume are considered, e.g., a solvent shell or a counterion, this area of occupation is consistent with that expected for a close packed monolayer in which the radius of the metal complex (crystallographic data¹³ indicate that the radii of osmium and ruthenium polypyridyl complexes are of the order of 6.7 Å), rather than the length of the bridging ligands, dictates the surface coverage. This area of occupation is smaller than that found for adsorbed [Os(bpy)₂Cl(p3p)]⁺ complexes⁷ (240 Å²) and is indistinguishable from that found

for adsorbed [Os(bpy)₂(pyridine)(p3p)]²⁺ complexes,¹⁴ both of which contain only one p3p bridging ligand. Molecular modeling of the [Os(bpy)₂(p3p)₂]²⁺ complex suggests that if both p3p ligands adsorbed onto the electrode surface, then its area of occupation would be at least 214 Å², a value that is approximately 30% larger than that experimentally observed. These observations suggest that only one of the p3p ligands is bound to the electrode surface. This conclusion is supported by our observation (vide infra) that the heterogeneous electron transfer rate constant k depends on the pH of the contacting electrolyte solution. This pH sensitivity of k contrasts with structurally related [Os(bpy)₂(pyridine)(p3p)]²⁺ monolayers where the heterogeneous electron transfer dynamics are independent of the solution pH.

As described previously,^{7,15} the ideality of the electrochemical response can be further probed by using chronocoulometry to determine the redox composition as a function of the applied potential.¹⁶ The slopes of plots of $\ln([\text{Ox}]/[\text{Red}])$ vs potential are independent of the pH, maintaining a value of 57 ± 3 mV/decade, as the pH of the contacting electrolyte solution is changed from 5.05 to 1.07. This slope is indistinguishable from those predicted for one electron transfer reactions by the Nernst equation,¹⁶ confirming that the thermodynamic aspects of electron transfer at these metal/monolayer interfaces are nearly ideal under the experimental conditions employed.

The formal potential for the Os^{2+/3+} redox reaction shifts from 0.638 to 0.654 V as the pH is systematically varied from 5.05 to 1.07. That $E^{\circ'}$ shifts in a positive potential direction indicates that protonation stabilizes the reduced state of the complex. This small shift in $E^{\circ'}$ is consistent with the methylene spacer groups preventing effective electronic communication between the two pyridine rings (vide infra). Moreover, the small shift in $E^{\circ'}$ suggests that the electrostatic effects of protonating the unbound pyridine ring are minor. This behavior probably arises because the high dielectric constant of water and the high supporting electrolyte concentration efficiently screen the charge on the pyridinium ion that is located 9–10 Å away from the osmium redox center.

Interfacial Capacitance. Probing the double layer capacitance C_{dl} gives an insight into the change in interfacial charge distribution that accompanies monolayer formation, the relative perfection of the monolayer, and perhaps its thickness.^{5,7,17} Here, we have used small amplitude potential step chronoamperometry to measure the interfacial capacitance as the electrolyte concentration was systematically varied. The potential step was centered at 0.100 V where the monolayer is redox inactive, and a pulse amplitude ΔE of 25 mV was employed. The pulse amplitude is sufficiently small to allow the measured capacitance to be regarded as an approximate differential capacitance. This potential step does not change the redox composition of the monolayer, and only single exponential decays due to double layer charging were observed. This capacitive current was analyzed using a plot of $\ln i_c(t)$ vs t to obtain the resistance R_u and double layer capacitance C_{dl} according to eq 1.¹⁸

$$i_c(t) = (\Delta E/R_u) \exp(-t/R_u C_{dl}) \quad (1)$$

For an electrochemical double layer, the differential capacitance increases with a decreasing separation between the electrode surface and the plane of closest approach for ionic charge and increases with increasing dielectric constant.¹⁶ There are two limiting cases for the potential profile across an adsorbed monolayer.⁵ First, the modified interface could be similar to a bare electrode so that all of the applied potential would be dropped close to the electrode/monolayer interface. In this case, the immobilized redox center would not experience a large

CHART 2

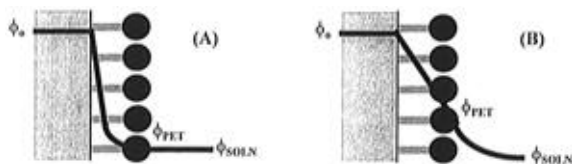


TABLE 1: Electrolyte Concentration Dependence of the Cell Time Constant $R_u C_{dl}$, Uncompensated Cell Resistance R_u , and Double Layer Capacitance C_{dl} as Measured at +0.100 V^a

[LiClO ₄], M	$R_u C_{dl}$, ns	$10^{-3}R_u$, Ω	C_{dl} , pF
0.02	266(18)	25.1(2.0)	10.6(1.0)
0.05	289(22)	18.3(1.8)	15.8(1.2)
0.10	195(8)	9.6(1.1)	20.4(1.8)
0.15	177(11)	7.1(0.6)	24.9(2.2)
0.21	150(10)	5.2(0.4)	28.7(2.4)
0.26	134(12)	4.1(0.4)	32.6(2.9)
0.29	114(9)	3.7(0.2)	30.8(3.0)
0.35	92(6)	3.1(0.3)	29.9(2.5)
0.40	95(7)	2.8(0.2)	34.5(3.2)
0.61	58(4)	1.8(0.1)	32.8(2.9)
0.80	41(3)	1.3(0.2)	31.7(3.1)
1.0	34(2)	1.1(0.1)	30.5(2.8)
1.2	29(2)	0.9(0.1)	32.8(2.5)

^a Numbers in parentheses represent the standard deviations for at least three individual monolayers. Supporting electrolyte is lithium perchlorate. The radius of the platinum microelectrode is 5 μm .

electric field (Chart 2A). Second, as discussed recently by Smith and White,^{5a} the existence of an impermeable monolayer that has a low dielectric constant may cause the potential to decay linearly across the thickness of the monolayer and then exponentially in the solution phase (Chart 2B). In this case, the surface-confined redox centers would experience a large electric field. An insight into the applicability of either model to our interfaces can be obtained by measuring the interfacial capacitance. This objective is doubly important because we are interested in the electric field effects on heterogeneous electron transfer, and the interaction of the highly charged protonated complexes with the interfacial electric field.

For the model illustrated in Chart 2B,¹⁹ the reciprocal total interfacial capacitance, C_T , is given by the sum of the reciprocal capacitances of the film, C_{film} , and the diffuse layer, C_{dif}

$$C_T^{-1} = C_{\text{film}}^{-1} + C_{\text{dif}}^{-1} \quad (2)$$

$$C_{\text{film}} = \epsilon_0 \epsilon_{\text{film}} / d \quad (3)$$

$$C_{\text{dif}} = \epsilon_0 \epsilon_{\text{SOLN}} \kappa \cosh[ze(\phi_{\text{PET}} - \phi_{\text{SOLN}}) / 2k_B T] \quad (4)$$

where ϵ_0 is the permittivity of free space, ϵ_{film} and ϵ_{SOLN} are the film and solution dielectric constants, respectively, d is the monolayer thickness, z is the charge number of the electrolyte ion, e is the absolute electronic charge, k_B is the Boltzmann constant, T is the absolute temperature, and ϕ_{PET} and ϕ_{SOLN} are the potentials at the plane of electron transfer and in the bulk solution, respectively (Chart 2). The quantity κ is given by $(2n^\circ z^2 e^2 / \epsilon_{\text{SOLN}} \epsilon_0 k_B T)^{1/2}$, where n° is the number concentration of the ions in solution.¹⁶

Only the diffuse layer capacitance depends on the potential or the concentration of supporting electrolyte. Therefore, the relative importance of that component may be probed by systematically varying the supporting electrolyte concentration and measuring the total capacitance. Table 1 contains the cell time constants, uncompensated cell resistances, and double layer capacitances as the concentration of LiClO₄ as supporting

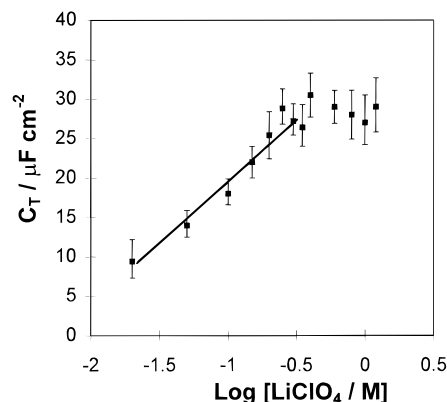


Figure 2. Dependence of the total interfacial capacitance for a spontaneously adsorbed (p3p)₂ monolayer on the logarithm of the supporting electrolyte concentration. The capacitance was determined using a small amplitude potential step centered on +0.100 V.

electrolyte is systematically varied from 0.02 to 1.2 M. Figure 2 shows the approximate differential capacitance, determined at 0.100 V, as a function of the logarithm of the supporting electrolyte concentration. The double layer capacitance increases approximately linearly with increasing logarithm of the electrolyte concentration for LiClO₄ concentrations less than about 0.2 M. This sensitivity clearly indicates that the diffuse layer capacitance contributes significantly to the total interfacial capacitance over this concentration range. The limiting value of C_T at high electrolyte concentration is at least 28 $\mu\text{F cm}^{-2}$, which may represent the film capacitance (Chart 2B), or if solvent and electrolyte ions freely diffuse into the interior of the monolayer and the double layer sets up as it would at a bare electrode (Chart 2A), it may correspond to the capacitance of the charges held at the outer Helmholtz plane. If this limiting capacitance is dominated by the film capacitance (Chart 2B), then, assuming a monolayer thickness of approximately 20 \AA , the relative dielectric constant within the film is estimated from eq 3 as 63. That the relative dielectric constant within the monolayer is comparable to that of water ($\epsilon_{\text{SOLN}} = 78.5$) would suggest that the monolayer is rather permeable to solvent and counterions.

Alternatively, the double layer may set up within the monolayer (Chart 2A), in which case the limiting interfacial capacitance corresponds to the capacitance of the charges held at the outer Helmholtz plane. Given that the distance of closest approach is likely to be of the order of 3 \AA , the relative dielectric constant within the double layer would have to decrease from the value of 78.5 for bulk water to approximately 9 before a limiting interfacial capacitance of 28 $\mu\text{F cm}^{-2}$ could be observed. It is important to note that, as discussed above for Chart 2B, this model is consistent with a solvated monolayer interior.

Therefore, based on these capacitance data, we conclude that the interior of the monolayer is at least partially solvated. This conclusion is consistent with the observation that the fwhm in cyclic voltammetry is close to that theoretically predicted for noninteracting redox sites, suggesting that solvent and ions permeate the monolayer and electrostatically insulate adjacent charges.

As described recently by Creager and co-workers,^{5b} an insight into the interfacial potential distribution, and hence monolayer permeability, can be obtained by probing the kinetics of heterogeneous electron transfer as the supporting electrolyte concentration is systematically varied. This is possible since a significant potential difference between the plane of the immobilized molecules and the bulk solution means that only

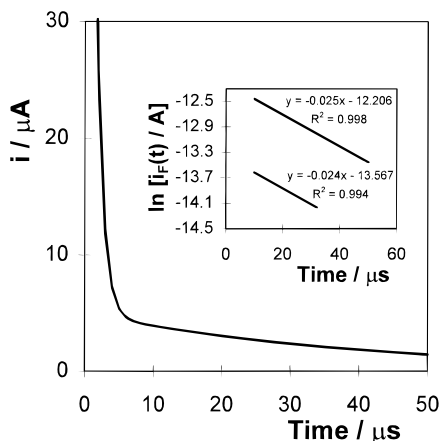


Figure 3. Current response for a 25 μm radius platinum microelectrode modified with a (p3p)₂ monolayer following a potential step where the overpotential η was -50 mV. The supporting electrolyte is 0.1 M perchlorate at a pH of 1.05. The inset shows $\ln i_F(t)$ vs t plots for the Faradaic reaction for a 25 μm (top) and a 12.5 μm (bottom) radius platinum microelectrode.

a fraction of the total interfacial drop drives the heterogeneous electron transfer process. In fact, the driving force would be governed by an equilibrium electrode potential that is a function of the electrostatic potential at the site for electron transfer. This means that the driving force for electron transfer changes as the redox reaction proceeds, causing the overall dynamics to deviate from first order kinetics.^{5b} We note that there are many processes other than interfacial fields that can cause nonexponential current decays, including multiple site geometries, surface activity effects,¹¹ the presence of defect sites,²⁰ oxidation state dependent dipole moments,²¹ or ion pairing.²² However, an increased supporting electrolyte decreases the double layer thickness κ , and if ions permeate into the monolayer, the situation is approached where all of the applied potential is dropped close to the electrode/monolayer interface. Therefore, one can probe the ideality of the chronoamperometric response without the complication of interfacial electric fields by employing high concentrations of supporting electrolyte.

Chronoamperometry. For an ideal electrochemical reaction involving a surface bound species, the Faradaic current following a potential step that changes the redox composition of the monolayer exhibits a single exponential decay in time according to^{3a,c,7}

$$i_F(t) = kQ \exp(-kt) \quad (5)$$

where k is the apparent rate constant for the overall reaction and Q is the total charge passed in the redox transformation.

Figure 3 illustrates a typical example of the chronoamperometric response observed for the reduction ($\text{Os}^{3+} + e^- \rightarrow \text{Os}^{2+}$) of a (p3p)₂ monolayer, where the electrolyte is 0.1 M aqueous LiClO_4 at a pH of 1.05. In this experiment the overpotential η ($\equiv E - E^\circ$) was -0.050 V. This figure shows that on a microsecond time domain two current decays can be separated. These responses, which arise from double layer charging and Faradaic current flow, are time-resolved due to the much shorter time constant of double layer charging compared to that of the Faradaic reaction. In our investigations, we have determined the electron transfer rate constant only when the time constant of double layer charging is at least five times shorter than the time constant of the Faradaic reaction.

While fast charging of the electrochemical double layer is important, the effects of ohmic losses must also be considered.¹⁶ When Faradaic and charging currents flow through a solution,

they generate a potential that acts to weaken the applied potential by an amount iR_u , where i is the total current. This ohmic drop can lead to severe distortions of experimental responses resulting in inaccurate measurements of the heterogeneous electron transfer rate. The significance of ohmic effects for these systems can be assessed using the data presented in Table 1. As illustrated in Figure 3, the Faradaic currents that flow in these high-speed chronoamperometric experiments are typically in the low-microamp range, even for 25 μm electrodes. Therefore, using the cell resistance data given in Table 1, the calculated iR_u drop is less than 20 mV for supporting electrolyte concentrations above 0.1 M. However, not only does the concentration of the supporting electrolyte play an important role in determining the magnitude of the uncompensated resistance, so too does the pH. For example, for the pH 1.05 system illustrated in Figure 3, the uncompensated resistance is approximately 2500 Ω , making the average ohmic loss approximately 5 mV.

The linearity of the $\ln i_F(t)$ vs t plot shown in the inset of Figure 3 indicates that electron transfer is characterized by a single rate constant over the time required to collect greater than 95% of the Faradaic charge. At supporting electrolyte concentrations greater than 0.1 M, the monolayers always gave linear first order decays over about two lifetimes. Deviations from linearity would be expected if ohmic drop was present. Uncompensated resistance causes the applied potential, and hence the apparent rate, to evolve with time. Therefore, iR_u drop produces negative deviations in the observed current at short times.⁷ That such nonidealities are not observed, at least for high concentrations of supporting electrolyte, is consistent with negligible ohmic losses. We have further probed the existence of ohmic effects by reducing the radius of the microelectrode. This approach is useful since the resistance increases with decreasing electrode radius, but the current decreases as the square of the radius leading to reduced ohmic effects for smaller electrodes. The inset in Figure 3 shows that the slope of the semilog plot obtained for a 12.5 μm platinum electrode modified with a spontaneously adsorbed (p3p)₂ monolayer is indistinguishable from that obtained at a 25 μm electrode. This observation is consistent with ohmic losses being negligible under the experimental conditions employed. Moreover, we find that the heterogeneous electron transfer rate constant measured at an overpotential of -50 mV is independent of the supporting electrolyte concentration, maintaining a value of $(2.5 \pm 0.2) \times 10^4 \text{ s}^{-1}$ as the LiClO_4 concentration was systematically varied from 0.1 to 1.0 M. On the basis of the measured cell resistances, and the insensitivity of the apparent heterogeneous rate constant to changes in electrode size or supporting electrolyte concentration, we conclude that ohmic drop and double layer effects on the interfacial kinetics are negligible for electrolyte concentrations greater than about 0.1 M.

Further evidence suggesting the predominance of a single rate constant is obtained by examining the intercept of the semilog plot at zero time. As indicated by eq 5, the intercept for a single exponential decay is $\ln(kQ)$. Nernst plots of the redox composition as a function of potential (vide supra) confirm that an absolute overpotential of 50 mV decreases the number of oxidized species within the monolayer to less than 10% of the total. Therefore, such a potential step effectively causes complete reduction of the film, and the full surface coverage, Γ , can be calculated from the intercept of Figure 3 using the relation¹¹

$$\Gamma = Q/nFA \quad (6)$$

where n is the number of electrons transferred, F is the Faraday

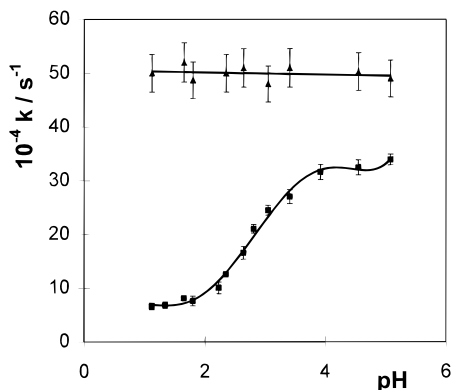


Figure 4. Dependence of the heterogeneous electron transfer rate constant at spontaneously adsorbed (p3p)₂ (lower curve) and [Os(bpy)₂(p3p)(pyridine)]²⁺ (upper line) monolayers on the pH of the contacting electrolyte. The supporting electrolyte concentration is approximately 0.1 M perchlorate. The overpotential η is 102 mV.

constant, and A is the real or microscopic electrode area. This chronoamperometric determination of the charge passed can then be compared with the value determined using cyclic voltammetry in order to further test the ideality of the chronoamperometric response. We find that the charges passed in these two independent experiments agree within 10%. This agreement indicates that all of the surface confined molecules are redox active on a microsecond time scale; i.e., relatively few, if any, sites are kinetically isolated.

Effect of Solution pH on Heterogeneous Kinetics. Plots of $\ln i_F(t)$ vs t , obtained at an overpotential of 102 mV, remain linear ($R^2 > 0.99$) as the pH of the contacting electrolyte solution is systematically varied from 5.05 to 1.07, and heterogeneous electron transfer rate constants have been evaluated from their slopes. Figure 4 shows that there is a sigmoidal relationship between the heterogeneous electron transfer rate constant and the pH of the electrolyte, with k decreasing from $(3.4 \pm 0.2) \times 10^5$ to $(6.6 \pm 0.4) \times 10^4$ s⁻¹ when the solution pH is decreased from 5.05 to 1.07. That k is sensitive to the solution pH, yet plots of $\ln i_F(t)$ vs t remain linear over a wide pH range, is significant. One might imagine that if the system were in two different states, protonated and nonprotonated, each with different rate constants, that the corresponding semilog plots would be nonlinear or, in the extreme case, would exhibit dual slope behavior. That such nonlinear behavior is not observed suggests that protonation equilibrium occurs more rapidly than redox equilibrium.

It is important to note that the cell resistance decreases as the pH of the electrolytic solution decreases. Therefore, one would expect ohmic effects to be more significant at high, rather than low, pH, which would cause the heterogeneous electron transfer rate constant to be underestimated at high pH. That the opposite trend is experimentally observed, i.e., k increases with increasing pH, supports our conclusion that ohmic effects do not adversely affect the chronoamperometric determination of k .

The inflection point of Figure 4 is located at a pH of approximately 2.9, which is consistent with the pK_a of the unbound p3p ligand.²³ These data suggest that protonating the unbound p3p ligand alters the rate of heterogeneous electron transfer across the electrode/monolayer interface. Figure 4 also shows that the rate of heterogeneous electron transfer to spontaneously adsorbed [Os(bpy)₂(pyridine)(p3p)]²⁺ monolayers, which do not contain groups capable of becoming protonated, is independent of solution pH in this range. This observation suggests that the second p3p ligand within the

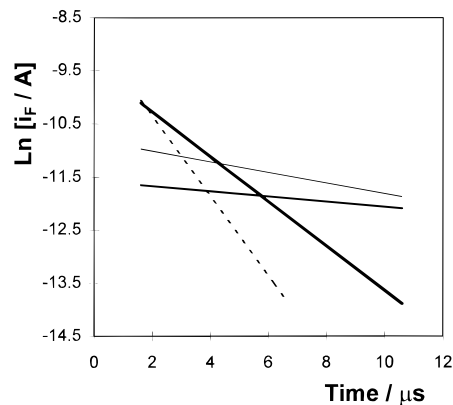


Figure 5. Effect of various overpotentials η , on the $\ln i_F(t)$ vs t plots for a spontaneously adsorbed (p3p)₂ monolayer. The supporting electrolyte is 0.1 M HClO₄. Taken on the right-hand side, the overpotentials are from top to bottom, 0.051, 0.103, 0.200, and 0.349 V, respectively.

coordination shell of the osmium complex plays a central role in making k sensitive to the solution pH.

A possible explanation of this pH dependence is that protonating the free pyridine ring of the p3p ligand alters the electron density on the redox center. However, the degree of electronic coupling between the pyridine rings of the p3p ligand is expected to be weak given that they are separated by three methylene spacer groups. Our experimental observation that the formal potential of the Os^{2+/3+} redox reaction remains constant to within 23 mV as the pH of the contacting solution is changed from 5.05 to 1.07 supports this conclusion. Moreover, solution phase absorption spectroscopy of the complex dissolved in DMF indicates that the position of the metal to ligand charge transfer band remains constant when the p3p ligands are protonated. This observation further suggests that protonation does not significantly affect the electron density on the osmium redox center.

The heterogeneous electron transfer rate is considered to depend on a frequency factor and a Franck–Condon barrier and can be expressed as²⁴

$$k = \Gamma_n \kappa_{el} v_n \exp(-\Delta G^\ddagger/RT) \quad (7)$$

where Γ_n is the nuclear tunneling factor, κ_{el} is the electronic transmission coefficient, v_n is the nuclear frequency factor, and ΔG^\ddagger is the free energy of activation.^{25,26} Since the experimental frequency factors are always less than $k_B T/h$ (h is the Planck constant), the nuclear tunneling factor is unity.²⁴ From eq 7, it is evident that the sensitivity of the heterogeneous electron transfer rate to the solution pH could be caused by changes in the free energy of activation or the pre-exponential factor. Since the free energy of activation equals $\lambda/4$, where λ is the total reorganization energy associated with switching the oxidation state of the monolayer, one strategy for estimating ΔG^\ddagger is to fit the dependence of the logarithm of the rate constant on the overpotential.^{2c,3a,c,27}

pH Effects on the Potential Dependence of k . Figure 5 illustrates the effect of various overpotentials on the $\ln i_F(t)$ vs t plots, where the supporting electrolyte is 0.1 M HClO₄. This figure shows that linear responses are observed at each of the overpotentials investigated. These linear responses are consistent with negligible ohmic effects despite the higher Faradaic currents that flow when a larger overpotential is applied. These data highlight another advantage of high-speed electrochemistry. As illustrated in Figure 1, the background current in cyclic voltammetry tends to rise as the positive potential limit is

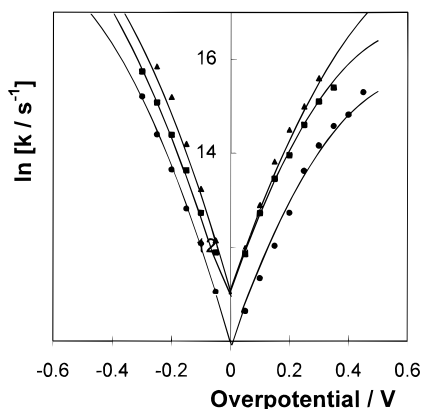


Figure 6. Tafel plots for (p3p)₂ monolayers as a function of the supporting electrolyte pH. The data (top to bottom, right hand side) represent electrolyte pH's of 5.05, 3.10, and 1.07, respectively. The solid lines denote theoretical fits obtained from a through-space tunneling model where $\lambda = 100, 68,$ and 56 kJ mol^{-1} from top to bottom, respectively. The errors are approximately equal to the size of the symbols.

TABLE 2: Effect of Electrolyte pH on Standard Heterogeneous Rate Constants, Activation Parameters, and Pre-exponential Factors^a

electrolyte pH	$\lambda,$ $10^{-4}k^{\circ},{}^b \text{ s}^{-1}$	$\Delta H^{\ddagger},$ kJ mol^{-1}	$\Delta G_c^{\ddagger},{}^c$ kJ mol^{-1}	$10^{-6}A_{\text{ets}},{}^d \text{ s}^{-1}$	
5.05	6.1(0.2)	100	37.5(2.1)	25.1(2.2)	1547(345)
3.95	6.0(0.2)	93	34.6(1.8)	22.1(1.7)	451(78)
3.10	4.3(0.1)	68	30.3(1.3)	17.0(0.9)	41(6)
2.08	2.0(0.1)	54	26.1(2.2)	13.8(1.4)	5.3(0.6)
1.07	1.6(0.1)	56	24.6(1.5)	14.3(1.1)	5.2(0.4)

^a Numbers in parentheses represent the standard deviations for at least three individual monolayers. Supporting electrolyte is 0.1 M perchlorate. ^b All standard rate constants were determined at 298 K. ^c Free energy of activation determined from the cathodic ideal electrochemical enthalpies using $\Delta S_{\text{rc}}^{\circ}$. ^d Pre-exponential factor extracted from the standard heterogeneous electron transfer rate constant using ΔG^{\ddagger} .

approached. This increasing background current arises from the initial electrochemical cleaning of the platinum surface and is caused by incomplete removal of adsorbed oxygen or platinum oxide. However, the processes responsible for these background currents appear to be slow and take place on a millisecond time scale. By probing the electron transfer dynamics on a microsecond time scale, these background currents can be effectively eliminated so that the chronoamperometric data are not affected even at overpotentials where the background in cyclic voltammetry may be rising.

Figure 6 illustrates Tafel plots of $\ln k$ vs overpotential, η , for monolayers in contact with perchlorate electrolytes at different pHs. For overpotentials less than about 200 mV, $\ln k$ depends approximately linearly on η . The standard heterogeneous electron transfer rate constant k° has been determined by linearly extrapolating $\ln k$ to zero overpotential, and Table 2 contains these data. However, at large overpotentials the response is clearly nonlinear, and the slopes decrease in magnitude with increasing overpotential in both the anodic and cathodic directions. In the conventional Butler–Volmer formulation of electrode kinetics,¹⁶ these slopes represent $(1 - \alpha_a)F/RT$ and $-\alpha_c F/RT$ for the oxidation and reduction reactions, respectively, where α_a is the anodic, and α_c the cathodic, transfer coefficient. Therefore, in contrast with the expectations of the Butler–Volmer formulation, Figure 6 suggests that the transfer coefficients are potential dependent. Furthermore, as reported previously for $[\text{Os}(\text{bpy})_2\text{Cl}(\text{p3p})]^+$ monolayers,^{27a} α_a tends toward zero more rapidly than α_c . The Marcus theory of

electron transfer predicts these nonlinear Tafel plots, because it includes a term that is quadratic in η in the rate equation.²⁸

Simplified models incorporating the basic concepts of the Marcus theory have been developed to model heterogeneous electron transfer across electrode/monolayer interfaces.^{3a,c} Chidsey has developed a model describing through-bond electron tunneling across metal/monolayer interfaces.^{3a} However, this model predicts that Tafel plots will be symmetric with respect to overpotential. That we experimentally observe larger cathodic than anodic heterogeneous electron transfer rate constants for a given absolute value of the overpotential suggests that through-bond electron tunneling is not an appropriate model for our system. Finklea and Hanshaw^{3c} have assembled a model describing through-space electron tunneling that predicts our experimental observation of asymmetric Tafel plots. In Finklea's model, the heterogeneous electron transfer rate constant is given by the integral over energy of three functions, namely, the Fermi function of the metal, the distribution of energy levels for acceptor or donor states in the monolayer (assumed to be Gaussian), and a rate parameter for electron tunneling at a given energy. In order to fit this model to the experimental data shown in Figure 6, estimates are required for the average barrier height to heterogeneous electron transfer, the total reorganization energy associated with switching the redox state of the monolayer, and the preintegral factor.

The average barrier height for electron tunneling at $[\text{Os}(\text{bpy})_2\text{Cl}(\text{pNp})]^+$ monolayers, where pNp is 4,4'-bipyridyl, 1,2-di(4-pyridyl)ethane or 4,4'-trimethylenedipyridine, has previously been estimated from the distance dependence of k° .^{27a} Given that the same bridging ligand is used here, we employ the same value of the average barrier height, 200 kJ mol^{-1} , in the present analysis. The total reorganization energy λ , dictates the degree of curvature in the Tafel plots. Therefore, λ was chosen so that there was satisfactory agreement between shapes of the theoretical Tafel plots and the experimental data. Finally, the preintegral factor was adjusted to give the experimental value of k° .

Figure 6 shows the experimental dependence of $\ln k$ on overpotential for solution pH's of 5.05, 3.10, and 1.07. This figure indicates that the degree of curvature of these Tafel plots depends on pH, suggesting that the reorganization energy depends on the extent of monolayer protonation. Figure 6 shows that satisfactory agreement between Finklea and Hanshaw's model and the experimental data is obtained when λ is 100, 68, and 56 kJ mol^{-1} for solution pH's of 5.05, 3.10, and 1.07, respectively. However, we note that the electron transfer dynamics can only be probed over a restricted range of overpotentials because of the rapid nature of the process. This restriction means that only limited confidence can be placed in these fitted values of the reorganization energy.

The Marcus theory can provide a theoretical estimate of the reorganization energy.²⁸ In the Marcus model, λ is considered to be the sum of an inner sphere and outer sphere component. The inner sphere component describes the distortion of bond angles and lengths accompanying electron transfer, while the outer sphere component reflects solvent reorganization effects. Crystallographic data demonstrate that switching the oxidation state of osmium and ruthenium polypyridyl complexes does not significantly change either the bond lengths or angles. This observation suggests that the inner sphere reorganization energy for this system is negligible, at least in the solid state. The outer sphere solvent reorganization energy λ_{OS} is given by

$$\lambda_{\text{OS}} = (e^2/2)(r^{-1} - R_e^{-1})(\epsilon_{\text{op}}^{-1} - \epsilon_{\text{SOLN}}^{-1}) \quad (8)$$

where e is the absolute electronic charge, r is the radius of the

metal complex (6.7 Å), R_e is the reactant-image distance, ϵ_{op} is the optical dielectric constant of water (5.5), and ϵ_{SOLN} is the static dielectric constant (78.5). As discussed previously,^{27a} we have neglected imaging effects, i.e., $R_e \rightarrow \infty$, in calculating the theoretical solvent reorganization energy. Equation 8 yields a solvent reorganization energy of 56.9 kJ mol⁻¹, which agrees with the value of 56 kJ mol⁻¹ obtained from fitting the data in Figure 6 when the monolayer is fully protonated. This observation suggests that the activation energy barrier to heterogeneous electron transfer at a protonated monolayer is dictated by solvent reorganization. In contrast, the experimental reorganization energy for nonprotonated monolayers (100 kJ mol⁻¹) is significantly larger than that predicted by eq 8 for solvent reorganization. There are a number of factors that may cause the activation barrier to heterogeneous electron to depend on the monolayer's state of protonation. For example, the interfacial potential distribution may be different with the higher ionic strength of the low-pH solutions causing the potential to drop more sharply at the electrode/monolayer interface. These differences in electric field strength may change the solvent or ion content of the film. It is important to note that the experimental semilog current vs time responses remain linear over the pH range investigated. The linearity of these responses suggests that diffusional processes; e.g., the motion of charge compensating counterions does not influence the rate of, or the barrier to, heterogeneous electron transfer. Alternatively, redox induced changes in the film structure, e.g., a change in the tilt angle θ (Chart 1), may accompany oxidation of the monolayer. This reorientation of the adsorbate could act as an "inner sphere" reorganization energy, making the experimental λ larger for nonprotonated monolayers.

In the Marcus theory, the free energy of activation ΔG^\ddagger is equal to $\lambda/4$. Therefore, while the largest heterogeneous electron transfer rate is observed for nonprotonated monolayers (Figure 4), this process is associated with the largest free energy of activation (Figure 6). If the pre-exponential factor of eq 7 did not change as the monolayer became protonated, then a higher free energy of activation would give a lower, not a higher, heterogeneous electron transfer rate. This is an important observation and suggests that changes in the pre-exponential factor with monolayer protonation cause the heterogeneous electron transfer to be pH sensitive.

To avoid the inherent inaccuracy of fitting Tafel plots over a limited potential range to estimate ΔG^\ddagger , and to obtain a more quantitative insight into the origin of the pH sensitivity of k , we have performed temperature-resolved measurements of the formal potential and heterogeneous electron transfer rate to independently probe the pH dependence of the activation entropy and enthalpy, respectively.

Reaction Entropies. One might anticipate that since protonating the monolayer changes its charge, the reaction entropy ΔS_{rc}° , quantifying the difference in entropy between the reduced and oxidized forms of the redox couple, would depend on the pH of the contacting electrolytic solution.²⁹ If ΔS_{rc}° was pH dependent, then it could explain the pH dependence of the free energy of activation suggested by Figure 6.

The reaction entropy has been determined using a nonisothermal cell by measuring the temperature dependence of the formal potential obtained from cyclic voltammetry as the pH of the contacting solution was systematically varied. As discussed by Weaver and co-workers, the temperature dependence of the formal potential can be expressed as^{29,30}

$$\Delta S_{rc}^\circ = F(\partial E^\circ/\partial T) \quad (9)$$

For all situations investigated, the formal potential shifts in a

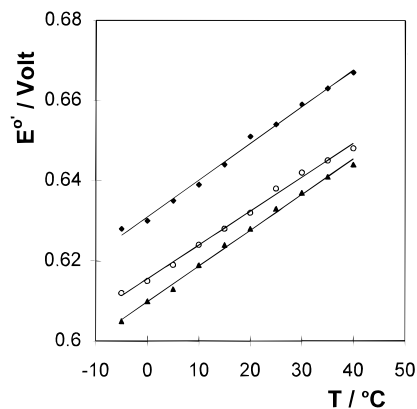


Figure 7. Effect of the pH of the contacting electrolyte solution on the temperature dependence of the formal potential for (p3p)₂ monolayers spontaneously adsorbed on platinum microelectrodes. The data represent (top to bottom) electrolyte pH's of 1.5, 5.2, and 3.6, respectively.

positive potential direction with increasing temperature indicating positive reaction entropies and a higher degree of local ordering in the oxidized than in the reduced state. Figure 7 shows that plots of E° vs T are linear over the pH range 5.2 to 1.5, and reaction entropies have been calculated from the slopes according to eq 9. The slopes of these lines do not depend on the pH of the contacting solution, and ΔS_{rc}° remains constant at 82 ± 7 J mol⁻¹ K⁻¹ over the pH range 5.2 to 1.5. This observation clearly demonstrates that changes in the activation entropy are not responsible for the pH dependence of the free energy of activation suggested by Figure 6.

Temperature Dependence of k . Weaver and co-workers³¹ have established that a temperature independent Galvani potential difference, ϕ_m , across the metal/solution interface can be achieved using a nonisothermal cell. The electrochemical activation enthalpy determined from an Arrhenius plot of $\ln k$ vs T^{-1} , where ϕ_m is held constant, has been termed "ideal",³² and we label it here as ΔH_1^\ddagger . For a reduction or cathodic reaction, this electrochemical activation enthalpy can be separated into "chemical", ΔH^\ddagger , and "electrical", $\alpha_c F \phi_m$, contributions according to

$$\Delta H_{1,c}^\ddagger = -R \left. \frac{\partial \ln k}{\partial (1/T)} \right|_{\phi_m} = \Delta H^\ddagger - \alpha_c F \phi_m \quad (10)$$

We have investigated the temperature dependence of the heterogeneous electron transfer rate using temperature-resolved chronoamperometry over the temperature range -5 to $+40$ °C. An overpotential of -50 mV, as determined at 298 K, was used throughout these experiments, and the resulting current–time transients were similar to those illustrated in Figure 3. The corresponding semilog plots were linear over approximately two lifetimes, and the heterogeneous electron transfer rate was evaluated from the slopes. In a typical set of experiments, the temperature was systematically varied over a range and then returned to the initial temperature. The same slope, $-k$, and intercept, $\ln(kQ)$, were observed within experimental error for the initial and final transients. This consistency indicates that cycling the temperature does not change the heterogeneous kinetics or the quantity of material immobilized on the electrode surface. The heterogeneous electron transfer rate constant increases with increasing temperature as anticipated for a thermally activated process. Arrhenius plots of $\ln k$ vs T^{-1} are linear ($R^2 > 0.995$) over the temperature range -5 to $+40$ °C. Table 2 contains the activation enthalpies, ΔH^\ddagger , obtained from the slopes of these plots after using the experimental transfer coefficient to correct for the electrical driving force (-50 mV)

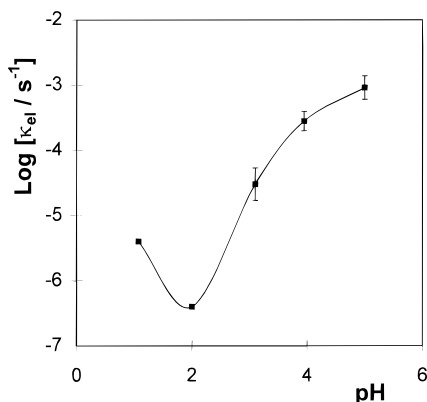


Figure 8. Dependence of the logarithm of the electronic transmission coefficient κ_{el} for heterogeneous electron transfer across platinum/(p3p)₂ monolayer interfaces on the pH of the supporting electrolyte.

according to eq 10. These data confirm that the activation enthalpy changes as the monolayer becomes protonated, decreasing from 37.5 ± 2.1 to 24.6 ± 1.5 kJ mol⁻¹ as the pH is reduced from 5.05 to 1.07.

In principle, it is possible to use the experimental enthalpies and entropies to calculate free energies of activation. Comparing these values with the value of the reorganization energy provided by Finklea and Hanshaw's model is an important test of consistency between these two independent experiments. We have calculated the cathodic free energy of activation according to eq 11,^{27a,32} and Table 2 contains the data. These data show that, at the five pH's investigated, ΔG_c^\ddagger and $\lambda/4$ agree to within 5%.

$$\Delta G_c^\ddagger = \Delta H_{I,c}^\ddagger - T\alpha_c \Delta S_{rc}^\circ \quad (11)$$

Pre-exponential Factor. That both ΔG_c^\ddagger and k decrease with decreasing electrolyte pH suggests that the pre-exponential factor of eq 7 decreases as the monolayer becomes protonated. Table 2 contains values of $A_{et} (\equiv \kappa_{el} v_n)$ that have been determined using our experimental free energies of activation and the standard heterogeneous electron transfer rate constant. To isolate the effects of the electronic transmission coefficient, we have calculated the nuclear frequency factor, v_n , using the dielectric continuum model,³³

$$v_n = \tau_1^{-1} (\Delta G_c^\ddagger / 4\pi k_B T)^{1/2} \quad (12)$$

where τ_1^{-1} is the inverse longitudinal relaxation time for water (1.9 ps⁻¹). These values have then been used to estimate κ_{el} from the experimental pre-exponential factor. Figure 8 shows that for all pH's investigated the electronic transmission coefficient is considerably less than unity. This observation indicates that there is a low probability of electron transfer once the nuclear transition state has been attained, suggesting a nonadiabatic reaction involving weak coupling between the metallic states of the electrode and the localized orbitals of the redox center. The pH dependency of $\log \kappa_{el}$ is illustrated in Figure 8. Significantly, κ_{el} increases dramatically from $(4.4 \pm 2.0) \times 10^{-6}$ to $(9.1 \pm 2.4) \times 10^{-4}$ on going from a protonated to a nonprotonated monolayer.

As discussed above, our observation of larger cathodic than anodic heterogeneous electron transfer rate constants for a given absolute value of the overpotential is consistent with through-space rather than through-bond electron tunneling. This is an important point since, unlike a through-space tunneling mechanism, the electron transfer distance for a through-bond tunneling process is not sensitive to the tilt angle (Chart 1) between

the electrode and the redox site. There are several possible causes of the observed dependence of the electronic transmission coefficient, and hence the heterogeneous electron transfer rate, on the pH of the contacting solution. For example, it is possible that at high pH immobilization occurs through both uncomplexed pyridine nitrogens and that lowering the solution pH causes desorption of one of the pyridine rings which then becomes protonated. We note however, that the experimental area of occupation as measured at high pH is considerably smaller than that predicted for the situation in which both uncomplexed pyridine groups bind to the electrode surface. Moreover, the pK_a's of both uncomplexed pyridines are identical, making selective desorption of one of them from the electrode surface unlikely. Alternatively, protonating the monolayer may either cause the tilt angle (Chart 1) between the bridging ligand and the electrode surface to increase, or the methylene spacer groups to adopt a more extended configuration. It is possible that this proton induced restructuring of the monolayer arises because the formal potential of the adsorbed complex is positive of the potential of zero charge. This situation is expected to cause repulsive interactions between the positively charged electrode and the highly charged protonated (4+) complexes, causing the redox centers to move away from the electrode and thus increasing the through-space tunneling distance.

If this model is appropriate, then the change in the through-space tunneling distance between the protonated and nonprotonated forms of the monolayer can be estimated from the data illustrated in Figure 8 by assuming that the tunneling parameter β° is identical to that found previously^{27a} for [Os(bpy)₂Cl(p3p)]⁺ monolayers (1.5 Å⁻¹). Using this value of β° , an increase in the through-space electron transfer distance of approximately 3.5 Å would be required to cause κ_{el} to decrease from $(9.1 \pm 2.4) \times 10^{-4}$ to $(4.4 \pm 2.0) \times 10^{-6}$ as the monolayer goes from a nonprotonated to a fully protonated state. When any directional component in the electronic coupling between the metallic states of the electrode and the orbitals of the adsorbed complex is ignored, this difference in through-space electron transfer distance could be accounted for by a change in the tilt angle from approximately 40° in the nonprotonated state to 90° in the protonated state.

Conclusions

The adsorbed monolayers considered here exhibit nearly ideal cyclic voltammetry and chronoamperometry as the pH, temperature, and experimental time scale are varied over a wide range. Chronoamperometry has been used to probe the rate of heterogeneous electron transfer across the monolayer/microelectrode interface. This process can be characterized by a single rate constant at high electrolyte concentrations, suggesting that heterogeneous electron transfer across these metal/monolayer interfaces is mechanistically uncomplicated. This unusual ideality has allowed us to probe the nature of the activation barrier to electron transfer, and the degree of electronic coupling between the remote redox centers and the microelectrode, in considerable detail. Measurements of the potential dependence of the heterogeneous electron transfer rate constant, k , suggest that electron transfer occurs via a through-space rather than a through-bond tunneling mechanism and that it depends on the pH of the contacting solution. By determining the free energy of activation using two independent methods, we have shown that changes in the pre-exponential factor rather than ΔG^\ddagger cause this pH sensitivity. It appears that the interaction of the highly positively charged protonated complexes with the interfacial electric field causes the through-space electron transfer distance to increase, perhaps by altering the tilt angle between the

adsorbate and the electrode surface or by causing the methylene spacer groups to become extended.

Although the change in heterogeneous electron transfer rate constant on going from nonprotonated to fully protonated monolayers is less than an order of magnitude, this pH induced "conformational gating" of the electron transfer rate offers the possibility of developing pH triggered electrical switches. We expect that fundamental investigations focusing specifically on the role that the local medium, particularly the bridging structure linking the reactants, plays in dictating the rate and pathway for electron transfer, will make it possible to design molecular systems that maximize electron transfer efficiency and their sensitivity to specific chemical triggers.

Acknowledgment. R.J.F. gratefully acknowledges Professor Larry R. Faulkner of the University of Illinois at Urbana-Champaign for the generous loan of the high-speed potentiostat used in this work. Financial support from Forbairt, the Irish Science and Technology Agency, under Basic Research Grant SC/95/209 is gratefully acknowledged.

References and Notes

- (1) (a) Abr na, H. D. In *Electroresponsive Molecular and Polymeric Systems*; Skoteim, T., Ed.; Dekker: New York, 1988. (b) Stoddart, J. F. In *Frontiers in Supramolecular Organic Chemistry and Photochemistry*; Schneider, H. J., D rr, H., Eds.; VCH: Weinheim, Germany, 1990. (c) Murray, R. W. *Molecular Design of Electrode Surfaces*; Wiley-Interscience: New York, 1992.
- (2) (a) Ulman, A. *An Introduction to Ultra-thin Organic Film from Langmuir-Blodgett to Self-Assembly*; Academic Press: San Diego, CA, 1991. (b) Chidsey, C. E. D.; Loiacono, D. N. *Langmuir* **1990**, *6*, 682. (c) Finklea, H. O.; Snider, D. A.; Fedik, J. *Langmuir* **1990**, *6*, 371. (d) Strong, L.; Whitesides, G. M. *Langmuir* **1988**, *4*, 546. (e) Nuzzo, R. G.; Dubois, L. H.; Allara, D. L. *J. Am. Chem. Soc.* **1990**, *112*, 558. (f) Yamada, S.; Kawazu, M.; Matsuo, T. *J. Phys. Chem.* **1994**, *98*, 3573. (g) Shi, X.; Caldwell, W. B.; Chen, K.; Mirkin, C. A. *J. Am. Chem. Soc.* **1994**, *116*, 11598.
- (3) (a) Chidsey, C. E. D. *Science* **1991**, *251*, 919. (b) Dudois, L. H.; Nuzzo, R. G. *Annu. Rev. Phys. Chem.* **1992**, *43*, 437. (c) Finklea, H. O.; Hanshew, D. D. *J. Am. Chem. Soc.* **1992**, *114*, 3173. (d) Acevedo, D.; Abr na, H. D. *J. Phys. Chem.* **1991**, *95*, 9590. (e) Acevedo, D.; Bretz, R. L.; Tirado, J. D.; Abr na, H. D. *Langmuir* **1994**, *10*, 1300. (f) Becka, A. M.; Miller, C. J. *J. Phys. Chem.* **1993**, *97*, 6233. (g) Rubinstein, I.; Steinberg, S.; Tor, Y.; Shanzer, A. *Nature* **1988**, *332*, 426. (h) Franzen, S.; Goldstein, R. F.; Boxer, S. G. *J. Phys. Chem.* **1993**, *97*, 3040. (i) Nordyke, L. L.; Buttry, D. A. *Langmuir* **1991**, *7*, 380. (j) Li, T. T.-T.; Weaver, M. J. *J. Am. Chem. Soc.* **1984**, *106*, 6107.
- (4) (a) Forster, R. *J. Chem. Soc. Rev.* **1994**, 289. (b) Faulkner, L. R.; Walsh, M. R.; Xu, C. *Contemporary Electroanalytical Chemistry*; Plenum Press: New York, 1990. (c) Andrieux, C. P.; Hapiot, P.; Sav ant, J. M. *Chem. Rev.* **1990**, *90*, 723. (d) Amatore, C. A.; Jutand, A.; Pfl ger, F. *J. Electroanal. Chem.* **1987**, *218*, 361. (e) Penner, R. M.; Heben, M. J.; Longin, T. L.; Lewis, N. S. *Science* **1990**, *250*, 1118. (f) Sabatani, E.; Rubinstein, I. *J. Phys. Chem.* **1987**, *91*, 6663.
- (5) (a) Smith, C. P.; White, H. S. *Anal. Chem.* **1992**, *64*, 2398. (b) Creager, S. E.; Weber, K. *Langmuir* **1993**, *9*, 844. (c) Andreu, R.; Fawcett, W. R. *J. Phys. Chem.* **1994**, *98*, 12753.
- (6) (a) Gao, J.; Shopes, R. J.; Wright, C. A. *Biochim. Biophys. Acta* **1990**, *1015*, 96. (b) Kaminskaya, O.; Konstaninov, A. A.; Shuvalov, V. A. *Biochim. Biophys. Acta* **1990**, *1016*, 153.
- (7) Forster, R. J.; Faulkner, L. R. *J. Am. Chem. Soc.* **1994**, *116*, 5444.
- (8) Yee, E. L.; Cave, R. J.; Guyer, K. L.; Tyma, P. D.; Weaver, M. J. *J. Am. Chem. Soc.* **1979**, *101*, 1131.
- (9) Xu, C. Ph.D. Thesis, University of Illinois at Urbana-Champaign, 1992.
- (10) Trasatti, S.; Petrii, O. A. *J. Electroanal. Chem.* **1992**, *327*, 354.
- (11) (a) Laviron, E. *J. Electroanal. Chem.* **1974**, *52*, 395. (b) Brown, A. P.; Anson, F. C. *Anal. Chem.* **1977**, *49*, 1589.
- (12) Feldberg, S. W.; Rubinstein, I. *J. Electroanal. Chem.* **1988**, *240*, 1.
- (13) (a) Goodwin, H. A.; Kepert, D. L.; Patrick, J. M.; Skelton, B. W.; White, A. H. *Aust. J. Chem.* **1984**, *37*, 1817. (b) Ferguson, J. E.; Love, J. L.; Robinson, W. T. *Inorg. Chem.* **1972**, *11*, 1662. (c) Rillema, D. P.; Jones, D. S.; Levy, H. A. *J. Chem. Soc., Chem. Commun.* **1979**, 849.
- (14) Forster, R. *J. Inorg. Chem.*, submitted for publication.
- (15) (a) Forster, R. *J. Langmuir* **1995**, *11*, 2247. (b) Forster, R. J.; Vos, J. G. *Langmuir* **1994**, *10*, 4330.
- (16) Bard, A. J.; Faulkner, L. R. *Electrochemical Methods: Fundamentals and Applications*; Wiley: New York, 1980.
- (17) (a) Bryant, M. A.; Crooks, R. M. *Langmuir* **1993**, *9*, 385. (b) Ksenzhek, O. S.; Petrova, S. A.; Oleinik, S. V.; Kokodyashnyi, M. V.; Moskovskii, V. Z. *Elektrokhim.* **1977**, *13*, 182. (c) Sun, L.; Johnson, B.; Wade, T.; Crooks, R. M. *J. Phys. Chem.* **1990**, *94*, 8869. (d) Porter, M. D.; Bright, T. B.; Allara, D. L.; Chidsey, C. E. D. *J. Am. Chem. Soc.* **1987**, *109*, 3559.
- (18) Wightman, R. M.; Wipf, D. O. In *Electroanalytical Chemistry*; Bard, A. J., Ed.; Dekker: New York, 1989; Vol. 15.
- (19) (a) Widrig, C. A.; Chung, C.; Porter, M. D. *J. Electroanal. Chem.* **1991**, *310*, 335. (b) Nuzzo, R. G.; Allara, O. L. *J. Am. Chem. Soc.* **1983**, *105*, 4481.
- (20) Chidsey, C. E. D.; Bertozzi, C. R.; Putvinski, T. M.; Mujsce, A. M. *J. Am. Chem. Soc.* **1990**, *112*, 4301.
- (21) Gerischer, H.; Scherson, D. A. *J. Electroanal. Chem.* **1985**, *188*, 33.
- (22) (a) Rowe, G. K.; Creager, S. E. *Langmuir* **1991**, *7*, 2307. (b) Nagamura, T.; Sakai, K. *Chem. Phys. Lett.* **1987**, *141*, 553. (c) Nagamura, T.; Sakai, K. *J. Chem. Soc., Faraday Trans.* **1988**, *84*, 3529. (d) Creager, S. E.; Rowe, G. K. *Anal. Chim. Acta* **1991**, *246*, 233.
- (23) Dean, J. A. *Handbook of Organic Chemistry*; McGraw-Hill: New York, 1987.
- (24) (a) Weaver, M. J. *Chem. Rev.* **1992**, *92*, 463. (b) Bagchi, G. *Annu. Rev. Phys. Chem.* **1989**, *40*, 115. (c) Sutin, N. *Acc. Chem. Res.* **1982**, *15*, 275.
- (25) Barr, S. W.; Guyer, K. L.; Li, T. T.-T.; Liu, H. Y.; Weaver, M. J. *J. Electrochem. Soc.* **1984**, *131*, 1626.
- (26) Sutin, N. *Brunschwig, B. S. ACS Symp. Ser.* **1982**, *198*, 105.
- (27) (a) Forster, R. J.; Faulkner, L. R. *J. Am. Chem. Soc.* **1994**, *116*, 5453. (b) Richardson, J. N.; Rowe, G. K.; Carter, M. T.; Tender, L. M.; Curtin, L. S.; Peck, S. P.; Murray, R. W. *Electrochim. Acta* **1995**, *40*, 1331.
- (28) (a) Marcus, R. A. *J. Chem. Phys.* **1956**, *24*, 966. (b) Marcus, R. A. *J. Chem. Phys.* **1965**, *43*, 679. (c) Tender, L. M.; Carter, M. T.; Murray, R. W. *Anal. Chem.* **1994**, *66*, 3173. (d) Weber, K.; Creager, S. E. *Anal. Chem.* **1994**, *66*, 3164.
- (29) Hupp, J. T.; Weaver, M. J. *J. Phys. Chem.* **1984**, *88*, 1860.
- (30) Barr, S. W.; Guyer, K. L.; Li, T. T.-T.; Liu, H. Y.; Weaver, M. J. *J. Electrochem. Soc.* **1984**, *131*, 1626.
- (31) (a) Li, T. T.-T.; Guyer, K. L.; Barr, S. W.; Weaver, M. J. *J. Electroanal. Chem.* **1984**, *164*, 27. (b) Yee, E. L.; Weaver, M. J. *Inorg. Chem.* **1980**, *19*, 1077.
- (32) (a) Weaver, M. J. *J. Phys. Chem.* **1979**, *83*, 1748. (b) Weaver, M. J. *J. Phys. Chem.* **1976**, *80*, 2645.
- (33) Morgan, J. D.; Wolynes, P. G. *J. Phys. Chem.* **1987**, *91*, 874.